Centrum voor Wiskunde en Informatica
REPORT*RAPPORT*

Coupling advection and chemical kinetics in a global atmospheric test model

E.J. Spee

Department of Numerical Mathematics

NM-R9508 1995

Report NM-R9508
ISSN 0169-0388

CWI
P.O. Box 94079
1090 GB Amsterdam
The Netherlands

Coupling Advection and Chemical Kinetics in a Global Atmospheric Test Model

E.J. Spee

CWI

P.O. Box 94079, 1090 GB Amsterdam, The Netherlands

Abstract

In this paper we consider the numerical difficulties that arise when horizontal advection is coupled with chemistry on a sphere, using operator splitting. From a numerical point of view, these two processes are the most difficult parts of an atmospheric model for global studies. The advection process is solved on a uniform grid and on a so-called reduced grid, where less cells are used near the poles than at the equator. The chemical kinetics is solved with Twostep, a solver based on the two-step backward differentiation formula, with constant and variable time steps. A reproducible test to measure the accuracy and the mass conservation property is introduced. To reduce the splitting error we integrate the chemistry along characteristics.

AMS Subject Classification (1991): Primary: 65M25. Secondary: 65M06, 80A30.
Keywords & Phrases: Hyperbolic PDEs; Linear advection; Chemical reactions; Global atmospheric models
Note: Background research for CIRK, a project with as goal the development of a global 3-D transport-chemistry model of the atmosphere. We gratefully acknowledge financial support from the RIVM.

1. Introduction.

Global atmospheric transport models are becoming increasingly important for the analysis and description of the distribution of trace gases and particles. Examples of these models are the GISS model of Jacob et al. [7], from which the TM2 model of Heimann and Keeling [3] was derived, and the Moguntia model of Zimmermann [15]. Important processes in these models are advection by wind and chemical kinetics. Other processes are deposition, emission and diffusion.

In this report horizontal advection and chemical kinetics on a sphere are described by

$$\frac{\partial c}{\partial t} + \frac{1}{a\cos\phi}\left[\frac{\partial(u\,c)}{\partial\lambda} + \frac{\partial(v\,c\cos\phi)}{\partial\phi}\right] = F(t,\,\lambda,\,\phi,\,c), \tag{1.1}$$

where c is a concentration vector with unit particles cm^{-3}, F is the operator describing the chemical kinetics, with unit particles $cm^{-3}\,s^{-1}$, u and v are the (given) wind velocity components in respectively the λ (longitude) and ϕ (latitude) direction and a is the radius of the earth, which is taken as a perfect sphere with radius $6378\,km$. In global models equation (1.1) is usually solved with operator splitting, such that advection and chemistry are handled with different numerical schemes and different time steps.

Desirable properties for the advection scheme are positivity, monotonicity and mass conservation combined with good shape preserving properties. We investigate the use of the unconditionally stable splitting scheme from [5] and a method of lines (MOL) scheme from [4]. Both schemes are provided with flux limiting to minimize oscillations and negative values. These schemes compare favorably with TREMBA and MPDATA [9]. On uniform grids the unconditional stability is attractive to avoid a too stringent CFL restriction emanating from the pole singularity [14]. However, the pole singularity also renders a stable scheme applied with large CFL number inaccurate. To overcome this difficulty, the

deformation correction proposed in [5] is applied. An alternative way to deal with the pole singularity is to use a so-called reduced grid [14], which coarsens the grid when approaching the poles. In this paper we use both a uniform and a reduced grid. The dimension splitting scheme and the MOL scheme are applied on a reduced grid in the manner proposed in [1].

The chemical solver must be computationally efficient in the 1% error range and preferably mass conservative. In this report, the chemical kinetics is solved with Twostep [11, 13], a solver based on the two-step backward differentiation formula, combined with Gauss-Seidel iteration to approximately solve the implicitly defined solution. For atmospheric chemistry problems Twostep compares favorably to QSSA [13] and VODE [12].

The research described in this paper deals on the one hand with the implementation of earlier derived advection schemes [1, 5] and on the other hand with the coupling between advection and chemical kinetics.

2. The numerical test problem.

We construct a test problem for which we can calculate a reference solution with an accuracy up to round-off error. For this purpose we use an analytical wind field, so that we can transform the PDE (1.1) into an ODE for all grid points by integrating along characteristics. These ODEs are solved with the state-of-the-art BDF code VODE [2]. The reference solution is calculated in double precision (14 decimal digits), all other calculations in single precision (7 decimal digits).

2.1 The wind field.

We use the wind velocities defined in [9]. These velocities describe a rotation over the globe, with an arbitrary angle β with the equator,

$$\begin{aligned} u(\lambda,\phi) &= (\cos\beta\cos\phi + \sin\beta\sin\phi\cos\lambda)\cdot\kappa, \\ v(\lambda,\phi) &= -\sin\beta\sin\lambda\cdot\kappa. \end{aligned} \tag{2.2}$$

We choose $\beta = 45^o$ to have a compromise between the most difficult numerical test ($\beta = 90^0$) and the prevalent wind ($\beta = 0^o$). In our test, we scaled the wind such that one rotation lasts 14 days, using

$$\kappa = \frac{a}{14 \times 24 \times 3600},$$

where a is the radius of the earth and the constant $14 \times 24 \times 3600$ is just 14 days in seconds. The unit of κ is $m\,s^{-1}$. With this wind field it is possible to exactly calculate the paths of an air packet in a Lagrangian calculation. That is, for each grid point equation (1.1) transforms into an ODE

$$\frac{dc}{dt} = F(t,\, \lambda^*(t),\, \phi^*(t),\, c). \tag{2.3}$$

The calculation of $\lambda^*(t)$ and $\phi^*(t)$ is given in Appendix B. In our tests we simulate one rotation which starts at day 181 at 00.00 hours.

2.2 Chemical model.

We use a Methane oxidation cycle which we obtained from Han The at the RIVM [10]. This model is used in long term global studies. The model has 17 non constant species, two lump species and 46 reactions, and is stiff. The model is fully described in [12] where it is tested as a box model. In the 2D test described in this report, we use realistic values for the solar zenith angle, which makes the chemistry time and space dependent. Due to the absence of day or night in the polar regions the different species grow to a maximum or decrease to a minimum. This gives sharp gradients at the

transition from polar region to the normal regions (see the concentration of N_2O_5 and NO in Figure 1) which makes the advection process difficult. Because the total number of N atoms is conserved in the

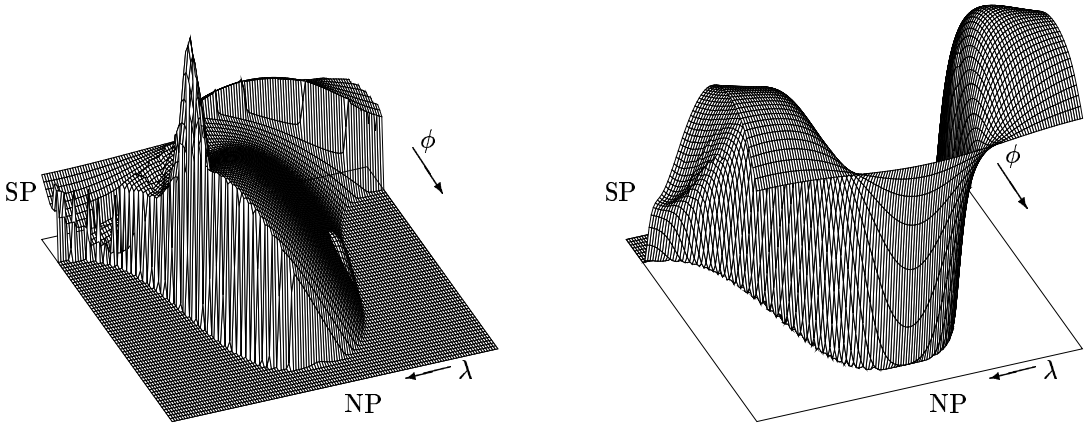

Figure 1: Concentration plot for N_2O_5 (left) and NO (right)

Methane oxidation cycle, we can test the conservation properties of the numerical scheme by summing all N atoms and comparing this with the sum of the initial value. All relevant information with respect to this chemical model can be found in `http://www.cwi.nl/ftp/edwins/CIRK_Prod_Loss.html` .

2.3 Initial concentration.
Numerical tests for advection schemes often use a constant background concentration disturbed with, e.g., a cone or a cylinder. If all components of the initial concentration would be shaped like that, the system would be far from chemical equilibrium. Therefore in our test run we use a background concentration that is in chemical equilibrium. This is achieved by starting a calculation at day 167 with over the whole earth the same concentration vector until we arrive at day 181. The initial concentration vector at day 167 is given in [12], Appendix B, Table 2. At day 181 we then add two cones on the concentrations of HNO_3 and NO to disturb the equilibrium. We use two cones, to have always one cone in the day zone and one in the night zone,

$$\begin{aligned} c(HNO_3;\, t,\, \lambda,\, \phi) &= c^*(HNO_3;\, t,\, \lambda,\, \phi) + 4.0 \times 10^9\; c_\gamma(\lambda,\, \phi) \\ c(NO;\, t,\, \lambda,\, \phi) &= c^*(NO;\, t,\, \lambda,\, \phi) + 1.0 \times 10^9\; c_\gamma(\lambda,\, \phi) \end{aligned} \tag{2.4}$$

with

$$c_\gamma(\lambda,\, \phi) \;=\; \max(0,\, 1 - \frac{r^{(1)}(\lambda,\, \phi)}{R},\, 1 - \frac{r^{(2)}(\lambda,\, \phi)}{R}),$$

where $R = 7\Delta\lambda$, with $\Delta\lambda$ the grid length in the λ direction, and

$$r^{(j)}(\lambda, \phi) = 2\{\cos^2\phi\, \sin^2[(\lambda - \lambda_j)/2] + \sin^2[(\phi - \phi_j)/2]\}^{\frac{1}{2}},$$

$(\lambda_j,\, \phi_j)$ are the coordinates of the center of the day and night zone cone. These coordinates are $(\frac{\pi}{2},\, 0)$, $(1\frac{1}{2}\pi,\, 0)$.

3. Numerical solver.

For the advection part of equation (1.1) explicit methods are usually more efficient than implicit ones. Because of the stiffness of the chemical model, the chemical kinetics requires an implicit method. To combine these methods we consider operator splitting.

3.1 Computational grid.
Computations are performed on two different grids, the well known uniform longitude latitude grid and a reduced grid. The specific reduced grid and data structure has been borrowed from [1]. The advantages of the reduced grid is a less severe CFL restriction at the poles, so that greater time steps can be made with standard explicit schemes. A favorable side effect is the reduction of the number of grid cells in which the chemical computations must be done. On the uniform grid in our test we use for the number of grid points in the λ and ϕ direction N_λ and N_ϕ respectively 128 and 64, resulting in a grid distance of 2.8125^o in both directions. For the reduced grid we double the latitude cell width at $|\phi| = 61.875^o, 75.9375^o, 84.375^o$, see Figure 2. This results in a minimum value for $\Delta\lambda \cos\phi$ which

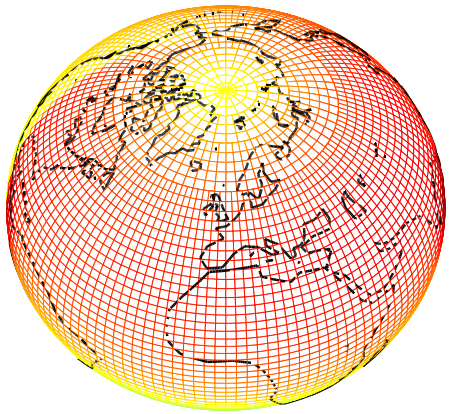

Figure 2: A reduced grid, with the coastline in illustration.

is circa 5.1 times smaller than the value at the equator. On a uniform grid this factor would be circa 40.9. The total number of grid points on a uniform grid amounts to 8192 versus 6304 on a reduced grid, which reduces the CPU time for the chemical computations with 23%.

3.2 Advection scheme.
The advection scheme Split-DeCo introduced in [5] is used on the uniform longitude latitude grid and on the reduced grid. The Split-DeCo scheme is made unconditionally stable by allowing the stencil to vary with the Courant numbers. When we have a large CFL number, this scheme is still stable, but near the poles the scheme is inaccurate due to the pole singularity. To overcome this difficulty, a deformation correction is applied, see details in [5]. The MOL scheme [4] is used on the reduced grid only. Both schemes use the same four-point, upwind biased stencil in each direction and are provided with flux limiting to minimize the occurrence of oscillations and negative values. The MOL scheme uses a 2-stage Runge-Kutta method for the time integration and hence is approximately two times more expensive for a given step size than the Split-DeCo scheme.

3.3 Chemical solver.
The chemical solver used is Twostep [11, 13]. Twostep is a stiff ODE-solver based on the 2nd-order implicit backward differentiation formula (BDF2). Twostep has been designed as a special purpose solver for atmospheric chemistry ODE problems and uses explicit Gauss-Seidel iteration for approximately solving the implicit relations. As in [12] we use NO_x and O_x lumping to enhance accuracy for a low number of iterations.

To avoid many rejected steps in Twostep caused by the sharp transitions at sunrise and sunset, we wrote a subroutine which calculates sunrise and sunset, and let Twostep restart at these times, see

Appendix C. The restart is accomplished by giving Twostep sunset or sunrise as the start or end of the integration interval, if occurring. In this case we can also restart when using constant time steps. In the full scale model we have in mind this restart might be also necessary for parametrizations which also strongly depend on the solar zenith angle.

3.4 The operator splitting technique.
Discretization of the advection operator in equation (1.1) yields an ODE system,

$$\frac{dc(t)}{dt} = A(t, c(t)) + F(t, \lambda, \phi, c(t)).$$

We use Strang splitting. Because the space-dependency of the solar zenith angle causes a splitting error, we improve Strang splitting for this case by integrating the chemistry along characteristics. For first order splitting this correction is proposed in [6]. Because of the startup costs of the chemical solver, we calculate the chemistry in the middle step to have a two times larger integration interval. Thus we use the splitting

$$\begin{aligned}
&\frac{dc^*(t)}{dt} = A(t, c^*(t)), && t_n \le t \le t_{n+\frac{1}{2}},\\
&&& c^*(t_n, \lambda, \phi) = c_n(\lambda, \phi),\\
&\frac{dc^{**}(t)}{dt} = F(t, \lambda + \frac{u}{a\cos\phi}(t - t_{n+\frac{1}{2}}), \phi + \frac{v}{a}(t - t_{n+\frac{1}{2}}), c^{**}(t)), && t_n \le t \le t_{n+1},\\
&&& c^{**}(t_n, \lambda, \phi) = c^*(t_{n+\frac{1}{2}}, \lambda, \phi),\\
&\frac{dc^{***}(t)}{dt} = A(t, c^{***}(t)), && t_{n+\frac{1}{2}} \le t \le t_{n+1},\\
&&& c^{***}(t_{n+\frac{1}{2}}, \lambda, \phi) = c^{**}(t_{n+1}, \lambda, \phi),
\end{aligned} \tag{3.5}$$

giving the new approximation at time level t_{n+1}.

The meteorological input used in the full scale model we have in mind is updated every 6 hours. This implies that the advection step should be 6 hours divided by an integer. Combined with the CFL condition in the ϕ direction for the Split-DeCo scheme on a uniform grid, this gives 224 advection steps for a full rotation. This makes the advection step $1.5\,h$ and the chemical integration interval $3\,h$. To have the same integration interval for the chemistry when using for advection the dimensional splitting scheme and the MOL scheme, we divided in the MOL scheme the advection step in 4 sub advection steps of $1.5/4\,h$ to maintain stability. This is essential for the comparison we make, because the length of the time interval $t_{n+1} - t_n$ determines the splitting error and the influence of the start up costs of the chemistry.

4. Numerical experiments.

4.1 Numerical experiment with the advection schemes.
The advection schemes are tested with a full rotation over both poles ($\beta = 90^o$). By way of comparison, we also apply the Donor Cell scheme. The advected concentrations are a cone with no background and maximum 0.9 (cone) and a cylinder with background 1.0 and maximum 2.0 (cyl). The number of advection steps (#adv) is for the Donor Cell 5120 (as in [9]), for the Split-DeCo 256 (as in [5]) and for the MOL scheme 1450 (the nearest even number as in [1], because of Strang splitting we want an even number). Notice that now $\beta = 90^o$ which necessitates a somewhat larger number of steps than necessary for $\beta = 45^o$. The results are given in Table 1, where EMIN and EMAX are respectively the

method	#adv	shape	EMIN	EMAX	ERR0	ERR1	CPU (s)	CPU' %
Donor Cell	5120	cone	0.0	-8.3E-1	6.3E-2	0.0	206	100.0
unif., Split-DeCo	256	cone	0.0	-1.5E-1	8.8E-3	-1.0E-3	20	9.8
red., Split-DeCo	256	cone	-2.2E-3	-1.8E-1	1.0E-2	-2.8E-3	22	10.9
red. MOL	1450	cone	-2.4E-6	-2.9E-1	1.6E-2	0.0	150	72.9
Donor Cell	5120	cyl	0.0	-3.0E-1	6.7E-2	0.0	206	100.0
unif., Split-DeCo	256	cyl	-2.3E-2	1.9E-2	2.8E-2	7.6E-5	20	9.8
red., Split-DeCo	256	cyl	-1.6E-2	2.3E-2	3.0E-2	6.1E-5	22	10.9
red. MOL	1450	cyl	-2.4E-3	1.3E-3	3.2E-2	0.0	150	72.9

Table 1: Results from a test with different advection schemes.

error of the minimum and the maximum value, ERR0 is the scaled L_2-error, and ERR1 is a measure for the mass balance. The errors are the same as in [5, 9],

$$\text{EMIN} = \frac{\min(c^n_{i,j}) - \min(c_{i,j}(t_n))}{\max(c_{i,j}(t_n))}, \qquad \text{EMAX} = \frac{\max(c^n_{i,j}) - \max(c_{i,j}(t_n))}{\max(c_{i,j}(t_n))},$$
$$\text{ERR0} = \frac{(\sum \gamma_j (c^n_{i,j} - c_{i,j}(t_n))^2)^{1/2}}{\max(c_{i,j}(t_n))}, \qquad \text{ERR1} = \frac{\sum \gamma_j c^n_{i,j}}{\sum \gamma_j c_{i,j}(t_n)} - 1,$$

where $\gamma_j = \cos(\phi_j)/(N_\lambda \sum_{k=1}^{N_\phi} \cos(\phi_k))$. The scaling is chosen such that ERR0 will be equal to 1 if the error is 1 in all grid points and $\max(c_{i,j}(t_n)) = 1$. The sums and max/min values are taken over $i = 1, \cdots, N_\lambda$, $j = 1, \cdots, N_\phi$. In all formulas $c_{i,j}(t_n)$ denotes the reference solution, and $c^n_{i,j}$ the computed solution at time t_n. CPU' is the relative CPU compared to the Donor Cell algorithm. The results are for double precision to overcome some difficulties caused by underflow due to numerical diffusion.

The ERR0 error of the Split-DeCo and the MOL scheme are of the same order of magnitude, and comparable with the errors of the scheme in [8], but this scheme seems to be more expensive in terms of computational effort. The MOL scheme uses more CPU time and is more diffusive, but is closer to physics as it uses no splitting. The Split-DeCo schemes are not strictly mass conservative, but the ERR1 error is acceptable. The schemes on a reduced grid are not positive, but this can easily be repaired in cases where positivity is very important, see Appendix A. The Split-DeCo scheme gives the best results, even on a uniform grid.

4.2 Numerical experiment with Twostep.

To examine the time step strategy in Twostep we have first integrated along characteristics, where errors are only caused by the chemical solver. We use 2 Gauss-Seidel iterations and in the tests with variable time steps between τ_{min} and τ_{max}, the relative tolerances (rtol) are 10^{-1}, 10^{-2} and 10^{-3}. The absolute tolerance is always 1.0. A lower bound of $\tau_{min} = 30\,s$ prevents Twostep from taking too small time steps. Increasing this lower bound is strongly dissuaded, because the BDF2 solution will then sometimes give unphysical negative concentrations. The results are given in Table 2, where L2(ERR0) is the L_2-error over the components over ERR0, the global L_2-error. $\overline{ERR1}$ is the mean over the components over ERR1 and is a measure for the mass balance.

Although variable time steps gives good results, we have also performed runs with constant time steps, because this will probably be more attractive when working on a vector machine. Then, $120\,s$ gives an optimum between CPU and accuracy for constant time steps, although the BDF2 solution then sometimes gives negative solutions. Using a constant time step of $30\,s$ in this test costs about 12 hours. Results for rtol $= 10^{-1}$ and $\tau_{min} = 30\,s$ gives for the lowest CPU time the desired accuracy of approximately 1%.

τ_{min} / τ_{max} (s)	rtol	L2(ERR0)	$\overline{ERR1}$	CPU (h)
1/900	1E-1	4.8E-3	9.0E-3	1.87
30/900	1E-1	4.8E-3	9.0E-3	1.72
1/900	1E-2	2.4E-3	4.5E-3	3.85
30/900	1E-2	2.4E-3	4.5E-3	2.13
1/900	1E-3	2.6E-4	4.6E-4	10.03
240/240	–	1.7E-2	2.9E-2	1.61
120/120	–	5.7E-3	9.6E-3	3.13
60/ 60	–	7.4E-4	1.4E-3	6.22

Table 2: Results from a test along characteristics.

method	τ_{min} / τ_{max} (s)	rtol	L2(ERR0)	L2(EMAX)	$\overline{ERR1}$	CPU (h)
unif. Split-DeCo	30/900	1E-1	8.7E-3	2.5E-2	8.5E-3	1.05
red. Split-DeCo	30/900	1E-1	8.9E-3	2.5E-2	8.4E-3	0.88
red. MOL	30/900	1E-1	9.6E-3	4.6E-2	8.3E-3	1.17
unif. Split-DeCo	1/900	1E-3	7.5E-3	3.1E-2	2.2E-4	6.21
red. Split-DeCo	1/900	1E-3	7.8E-3	3.1E-2	2.2E-4	5.59
red. MOL	1/900	1E-3	8.6E-3	5.3E-2	1.5E-4	5.82

Table 3: Advection with chemical kinetics on a uniform and a reduced grid.

4.3 Advection and chemical kinetics.

In Table 3 we show the results of coupling the Split-DeCo scheme and the MOL scheme with Twostep using variable time steps. We use the same errors as in Table 2, extended with an error measure representing smearing, L2(EMAX), the L_2-error over the components over EMAX, the error in the maximum.

In all cases the mass balance error is mainly determined by the chemistry solver, whereas the smearing is mainly determined by the advection solver. The global L_2-error over all components is caused by the operator splitting, the advection solver and the chemistry solver, although in the case with the most accurate chemistry, this term is negligible. The Split-DeCo scheme on a reduced grid gives for the lowest CPU the desired accuracy. The MOL scheme on a reduced grid costs more CPU time and is more diffusive.

In Table 4 results are given for a test without a restart at sunset and sunrise, and results for a calculation without integrating chemistry along the characteristics. The advection is carried out with the Split-DeCo scheme on a uniform grid. From this table it is clear that a restart at sunrise and sunset is redundant. On the other hand, integration along characteristics reduces the global L_2-error from approximately 1.4% to 0.8%, without extra CPU time.

Figure 3 and 4 are plots for the sum of N-atoms, after a full rotation on a reduced grid. There is no splitting error visible at the poles with the Split-DeCo scheme, and it is clear that the MOL approach is somewhat more diffusive, in accordance with the tests presented in [5, 4].

5. Results and conclusions.

The tests described in this report show that the reduced grid is a good approach to reduce CPU, while maintaining accuracy. However, they reveal that the Split-DeCo scheme also performs very satisfactorily on the uniform grid due to the possibility to apply this scheme unconditionally stable

restart	along characte-ristics	τ_{min} / τ_{max} (s)	rtol	L2(ERR0)	L2(EMAX)	$\overline{ERR1}$	CPU (h)
yes	yes	1/900	1E-3	7.5E-3	2.8E-2	2.4E-4	6.21
no	yes	1/900	1E-3	7.5E-3	3.1E-2	2.7E-4	6.23
yes	no	1/900	1E-3	1.3E-2	2.9E-2	1.5E-3	6.32
no	no	1/900	1E-3	1.3E-2	2.9E-2	1.5E-3	6.46
yes	yes	30/900	1E-1	8.7E-3	2.5E-2	8.5E-3	1.05
no	yes	30/900	1E-1	8.7E-3	2.5E-2	8.6E-3	1.09
yes	no	30/900	1E-1	1.4E-2	2.4E-2	9.0E-3	1.02
no	no	30/900	1E-1	1.4E-2	2.4E-2	9.1E-3	1.05
yes	yes	120/120	–	9.6E-3	2.4E-2	1.1E-2	2.31
no	yes	120/120	–	9.7E-3	2.3E-2	1.1E-2	2.28
yes	no	120/120	–	1.5E-2	2.2E-2	1.4E-2	2.26
no	no	120/120	–	1.5E-2	2.2E-2	1.4E-2	2.27

Table 4: Effect of restart and integration along characteristics.

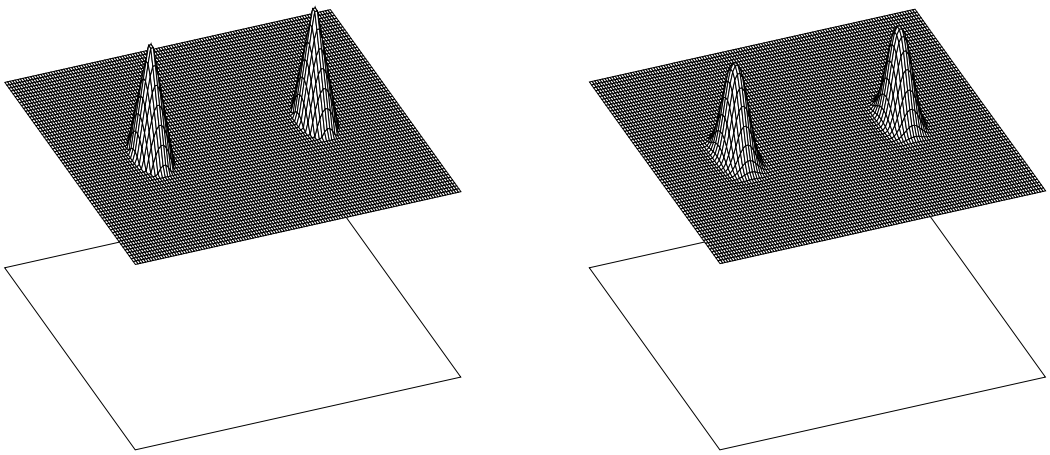

Figure 3: Reference solution (left) and redgridDeCo (right)

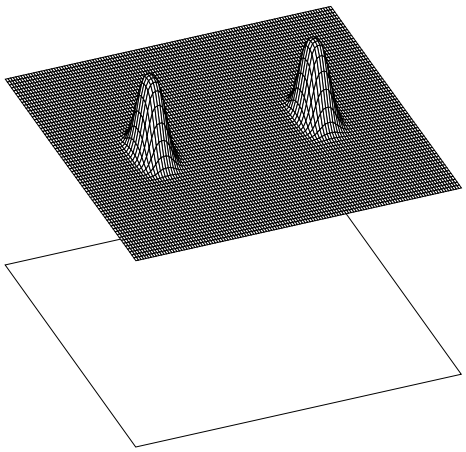

Figure 4: Results for the MOL approach.

at the poles, as suggested in [5]. On the other hand, for the MOL scheme grid reduction is necessary for coping with singularities at the poles.

On the scalar machine used here, variable time steps in the chemistry solver gives the best results. We will test in the near future whether this is also valid on vector and parallel machines. All combinations of schemes in this report give the desired accuracy of approximately 1%, see Tables 3 and 4, except the smearing for the MOL scheme. The CPU time for the Split-DeCo scheme is dominated by the chemistry. In the MOL approach the CPU time is caused for roughly 63% by the chemistry and for 37% by the advection. The MOL approach costs roughly 33% more CPU than the Split-DeCo approach and is more diffusive. Coupled with chemistry, the Split-DeCo scheme performs well on both a uniform and a reduced grid. The splitting error caused by the time splitting of the advection and chemistry is about 0.6% for the split step size of $3\,h$. This error can be reduced by integrating chemistry along characteristics.

References

1. J. G. Blom, W. Hundsdorfer, and J. G. Verwer. Vectorization aspects of a spherical advection scheme on a reduced grid. Report NM-R9418, CWI, Amsterdam, 1994.
`http://www.cwi.nl/ftp/CWIreports/NW/NM-R9418.ps.Z` .
2. P. N. Brown, G. D. Byrne, and A. C. Hindmarsh. VODE: A variable coefficient ODE solver. *SIAM J. Sci. Stat. Comput.*, 10:1038–1051, 1989.
3. M. Heimann and C. D. Keeling. A three-dimensional transport model for atmospheric CO_2: 2. model description and simulated tracer experiments. In D. H. Peterson, editor, *Aspects of climate variability in the pacific and the Western Americas, Geophysicial monograph 55*, pages 237–275. AGU Washington, 1989.
4. W. Hundsdorfer, B. Koren, M. van Loon, and J. G. Verwer. A positive finite-difference advection scheme. *J. Comput. Phys.*, 117:35–46, 1995.
`http://www.cwi.nl/ftp/gollum/AfAF_papers/NM-R9309.ps.Z` .
5. W. Hundsdorfer and E. J. Spee. Dimensional splitting with unconditional stability for advection on a sphere. Report NM-R9416, CWI, Amsterdam, 1994.
`http://www.cwi.nl/ftp/gollum/AfAF_papers/NM-R9416.ps.Z` .
6. W. Hundsdorfer and J. G. Verwer. A note on splitting errors for advection-reaction equations. Report NM-R9424, CWI, Amsterdam, 1994.
`http://www.cwi.nl/ftp/gollum/AfAf_papers/NM-R9424.ps.Z` .
7. D. J. Jacob, M. J. Prather, S. C. Wofsy, and M. B. McElroy. Atmospheric distribution of ^{85}Kr simulated with a general circulation model. *J. Geophys. Res.*, 92:6614–6626, 1987.
8. P. J. Rasch. Conservative shape-preserving two-dimensional transport on a spherical reduced grid. *Mon. Wea. Rev.*, 122:1337–1350, 1994.
9. P. K. Smolarkiewicz and P. J. Rasch. Monotone advection on the sphere: an Eulerian versus semi-Lagrangian approach. *J. Atmos. Sci.*, 48:793–810, 1991.
10. H. The. RIVM, Bilthoven, 1994. Private Communication.
11. J. G. Verwer. Gauss-Seidel iteration for stiff ODEs from chemical kinetics. *SIAM J. Sci. Comput.*, 15:1243–1250, 1994.
`http://www.cwi.nl/ftp/gollum/AfAF_papers/NM-R9315.ps.Z` .
12. J. G. Verwer, J. G. Blom, M. van Loon, and E. J. Spee. A comparison of stiff ODE solvers for atmospheric chemistry problems. Report NM-R9505, CWI, Amsterdam, 1995.
`http://www.cwi.nl/ftp/CWIreports/NW/NM-R9505.ps.Z` .
13. J. G. Verwer and D. Simpson. Explicit methods for stiff ODEs from atmospheric chemistry. Report NM-R9409, CWI, Amsterdam, 1994. (to appear in Appl. Numer. Math.)
`http://www.cwi.nl/ftp/gollum/AfAF_papers/NM-R9409.ps.Z` .
14. D. L. Williamson. Review of numerical approaches for modeling global transport. In H. van Dop and G. Kallos, editors, *Air Pollution Modeling and Its Application IX*. Plenum Press, New York, 1992.
15. P. H. Zimmermann. *Ein dreidimensionales numerisches Transportmodell für atmosphärische Spurenstoffe*. PhD thesis, Fachbereich Physik der Johannes Gutenberg - Universität, Mainz, 1984.

Centrum voor Wiskunde en Informatica
REPORT*RAPPORT*

Coupling advection and chemical kinetics in a global atmospheric test model

E.J. Spee

Department of Numerical Mathematics

NM-R9508 1995

Report NM-R9508
ISSN 0169-0388

CWI
P.O. Box 94079
1090 GB Amsterdam
The Netherlands

A. Implementation of the reduced grid.

Comments on the implementation of the reduced grid are from [1].

The reduced grid is implemented in a domain decomposition fashion where uniform blocks of different latitude cell widths are connected. At the interfaces the required concentrations are obtained by interpolation. To preserve mass conservation we impose as boundary conditions for the coarser blocks the fluxes computed on the boundary of the neighboring finer domains. If we assume one grid coarsening at $\phi_{J+\frac{1}{2}}$, and consequently also at $\phi_{N_\phi - J+\frac{1}{2}}$, we would get the following implementation:

- First handle the equatorial area, i.e., compute the fluxes for $i = 1, \cdots, N_\lambda$ and $j = J+1, \cdots, N_\phi - J$. If values c_{iJ} or $c_{iN_\phi - J+1}$ are needed they are obtained by linear interpolation from the available values

$$\begin{array}{rcll} c_{ij} & = & (3c_{\frac{i}{2}j} + c_{\frac{i}{2}+1j})/4, & i \text{ even} \\ c_{ij} & = & (3c_{\frac{i}{2}+1j} + c_{\frac{i}{2}j})/4, & i \text{ odd} \end{array} \tag{A.6}$$

- Next, compute the fluxes at the boundary for the South-Pole area

$$\begin{array}{rcl} \mathrm{fP}_{iJ+\frac{1}{2}} & = & (\mathrm{fP}_{2i-1J+\frac{1}{2}} + \mathrm{fP}_{2iJ+\frac{1}{2}})/2 \\ \mathrm{fP}_{i\frac{1}{2}} & = & 0, \qquad \text{for } i = 1, \cdots, N_\lambda/2 \end{array}$$

- Finally, compute the the fluxes at the boundary for the North-Pole area

$$\begin{array}{rcl} \mathrm{fP}_{iN_\phi - J+\frac{1}{2}} & = & (\mathrm{fP}_{2i-1N_\phi - J+\frac{1}{2}} + \mathrm{fP}_{2iN_\phi - J+\frac{1}{2}})/2 \\ \mathrm{fP}_{iN_\phi+\frac{1}{2}} & = & 0, \qquad \text{for } i = 1, \cdots, N_\lambda/2 \end{array}$$

The implementation for more domains is analogous.

The spatial discretization scheme implemented as above can result in negative values. This can be avoided by taking constant interpolation at the boundary of coarse to finer blocks, instead of linear interpolation. That means that equation (A.6) is replaced by

$$\begin{array}{rcll} c_{ij} & = & c_{\frac{1}{2}j}, & i \text{ even} \\ c_{ij} & = & c_{\frac{1}{2}+1j,}, & i \text{ odd} \end{array} \tag{A.7}$$

This leads to an order reduction at the boundary of coarse to finer blocks. After several tests we have done so far, it is not clear whether positivity is more important than the influence of the order reduction.

B. Exact solution of the advection.

In this section we calculate the position of a vector (λ_0, ϕ_0) at time τ, the time divided by the time of a full rotation, after being advected by the velocities given in equation (2.2) from [9],

$$\begin{aligned} u &= (\cos\beta\,\cos\phi + \sin\beta\,\sin\phi\,\cos\lambda)\cdot\kappa \\ v &= -\sin\beta\,\sin\lambda\cdot\kappa. \end{aligned}$$

These velocities describe a rotation over the earth with an angle β with the equator. The exact solution is a translation in a shifted coordinate system, which we denote with $\overline{x}, \overline{y}, \overline{z}$ (cartesian) and $\overline{\lambda}, \overline{\phi}$ (polar). For simplicity we use coordinates in which the radius of the earth is scaled to 1. We first translate the coordinates λ_0 and ϕ_0 into $\overline{\lambda_0}$ and $\overline{\phi_0}$,

$$\begin{aligned} x_0 &= \cos\phi_0\,\cos\lambda_0 \\ y_0 &= \cos\phi_0\,\sin\lambda_0 \\ z_0 &= \sin\phi_0 \\ \overline{x_0} &= z_0\,\sin\beta + x_0\,\cos\beta \\ \overline{y_0} &= y_0 \\ \overline{z_0} &= z_0\,\cos\beta - x_0\,\sin\beta \\ \overline{\phi_0} &= \arcsin(\overline{z_0}) \\ \overline{\lambda_0} &= \arctan2\pi(\overline{y_0}, \overline{x_0}), \end{aligned} \tag{B.8}$$

with $\arctan2\pi(y,\, x)$ is defined as

$$\begin{aligned} \arctan2\pi(y,\, x) &= \operatorname{atan2}(y/x) && \operatorname{atan2}(y/x) \geq 0 \\ \arctan2\pi(y,\, x) &= \operatorname{atan2}(y/x) + 2\,\pi && \text{elsewhere.} \end{aligned} \tag{B.9}$$

In this system we can calculate the rotation in one time step due to the wind.

$$\overline{\lambda_\tau} = \overline{\lambda_0} + \tau\,2\,\pi \quad \text{and} \quad \overline{\phi_\tau} = \overline{\phi_0}. \tag{B.10}$$

Finally we translate the rotated coordinates back in the original coordinate system.

$$\begin{aligned} \overline{x_\tau} &= \cos\overline{\phi_\tau}\,\cos\overline{\lambda_\tau} \\ \overline{y_\tau} &= \cos\overline{\phi_\tau}\,\sin\overline{\lambda_\tau} \\ \overline{z_\tau} &= \sin\overline{\phi_\tau} \\ x_\tau &= -\overline{z_\tau}\,\sin\beta + \overline{x_\tau}\,\cos\beta \\ y_\tau &= \overline{y_\tau} \\ z_\tau &= \overline{z_\tau}\,\cos\beta + \overline{x_\tau}\,\sin\beta \\ \phi_\tau &= \arcsin(z_\tau) \\ \lambda_\tau &= \arctan2\pi(y_\tau,\, x_\tau). \end{aligned} \tag{B.11}$$

C. Sunrise and sunset.

In this section we calculate sunset and sunrise because we want to restart the chemistry solver at sunset and sunrise by giving sunset or sunrise as the start or end of the integration interval. In a Lagrangian calculation we try to take the translation by wind into this calculation.

Given a start location (λ_0, ϕ_0) at t_0 and a local velocity (u, v) in $rad\,/\,h$, we will calculate the root of Equation (B.4) from [12], Appendix B.

$$\cos(Z) \;=\; \sin\Delta\,\sin\phi^*(t) \;+\; \cos\Delta\,\cos\phi^*(t)\,\cos\left(\frac{12\,h\;-\;tod(t,\,\lambda^*(t))}{12\,h}\pi\right) \;\equiv\; 0. \tag{C.12}$$

In contrast to the test in [12], two formulas are replaced by standard astronomical formulas. The time of day *tod* is replaced by the local solar time,

$$tod \;=\; \frac{t}{3600} \;+\; 12\,\frac{(\lambda\;-\;\pi)}{\pi},$$

where t is the model time, which is equal to the solar time at $\lambda = \pi$, both in hours. Let d be the day in the year $(1 \le d < 365)$. The declination Δ is given by

$$\begin{aligned}\Delta \;=\; & 0.396^o - 23.264^o\cos\left(\;(d+10.10\;\times\;2\,\pi)/365\right)\\ & -\;0.391^o\cos(2\,(d+\;\;3.88\;\times\;2\,\pi)/365)\\ & -\;0.176^o\cos(3\,(d+14.58\;\times\;2\,\pi)/365).\end{aligned}$$

The position vector as a function of time is given by

$$(\lambda^*(t),\,\phi^*(t)) \;=\; (\lambda_0 \;+\; u\,(t\;-\;t_0),\,\phi_0 \;+\; v\,(t\;-\;t_0)\,) \tag{C.13}$$

This holds for velocities which are almost constant along the trajectory. After substitution of the above equations in equation (C.12) we obtain

$$\begin{aligned}&\sin\Delta\,\sin\{\phi_0 \;+\; v\,(t\;-\;t_0)\}\;+\\ &\cos\Delta\,\cos\{\phi_0 \;+\; v\,(t\;-\;t_0)\}\;\times\\ &\cos\left(\left\{12\,h\;-\;\left\{t\;+\;\frac{12\,h}{\pi}\,(\lambda_0\;+\;u\,(t\;-\;t_0)\;-\pi)\right\}\right\}\frac{\pi}{12\,h}\right)\;\equiv\;0\end{aligned} \tag{C.14}$$

By using $\cos(2\,\pi\;-\;x)\;=\;\cos(x)$ we can simplify this equation in

$$\begin{aligned}\Rightarrow\quad &\sin\Delta\,\sin\{\phi_0 \;+\; v\,(t\;-\;t_0)\}\;+\\ &\cos\Delta\,\cos\{\phi_0 \;+\; v\,(t\;-\;t_0)\}\,\cos\left(\frac{\pi}{12\,h}\,t\;+\;\lambda_0\;+\;u\,(t\;-\;t_0)\right)\equiv\;0\end{aligned} \tag{C.15}$$

This is exactly solvable if $v \;=\; 0$

$$\begin{aligned}&\frac{\pi}{12\,h}\,t\;+\;\lambda_0\;+\;u\,(t\;-\;t_0) = \;\pm\,\arccos(-\tan\Delta\,\tan\phi_0),\;mod\,2\,\pi\\ &\Rightarrow t\;=\;\frac{u\,t_0\;-\;\lambda_0\;\pm\arccos(-\tan\Delta\,\tan\phi_0)}{\frac{\pi}{12\,h}\;+\;u},\;mod\,\frac{2\,\pi}{\frac{\pi}{12\,h}\;+\;u}\end{aligned} \tag{C.16}$$

In the case that v cannot be neglected in the calculation of sunrise and sunset, we use the time obtained with equation (C.16) for the next approximation. We have

$$\begin{aligned}F(u,\,v,\,t)\quad &=\;\sin\Delta\,\sin\{\phi_0\;+\;v(t\;-\;t_0)\}\\ &\quad+\;\cos\Delta\,\cos\{\phi_0\;+\;v(t\;-\;t_0)\}\,\cos(\frac{\pi}{12h}t\;+\;\lambda_0\;+\;u(t\;-\;t_0)),\end{aligned} \tag{C.17}$$

which is a function of t with constant parameters u, v. We want an approximation for a time t_2 with the property $F(u,\,v,\,t_2)\;=\;0$. This time can be approximated with

$$t_2 \approx t_1 - \frac{F(u, v, t_1)}{\left[\frac{\partial F}{\partial t}\right]_{t_1}} \tag{C.18}$$

where t_1 is the time with the property $F(u, 0, t_1) = 0$, and the partial derivative $\frac{\partial F}{\partial t}$ is given by

$$\begin{aligned}\frac{\partial F}{\partial t} &= \sin\Delta \cos\{\phi_0 + v(t - t_0)\} \cdot v \\ &+ \cos\Delta\Big\{-\sin\{\phi_0 + v(t - t_0)\} \cdot v \cdot \cos\Big(\frac{\pi}{12h}t + \lambda_0 + u(t - t_0)\Big) \\ &+ \cos\{\phi_0 + v(t - t_0)\} \cdot -\sin\Big(\frac{\pi}{12h}t + \lambda_0 + u(t - t_0)\Big) \cdot \{\frac{\pi}{12h} + u\}\Big\}.\end{aligned} \tag{C.19}$$